Structure and dynamics of *n*-alkanes confined by solid surfaces. I. Stationary crystalline boundaries

M. W. Ribarsky and Uzi Landman

School of Physics, Georgia Institute of Technology, Atlanta, Georgia 30332

Structural and dynamical properties of *n*-hexadecane films confined between two crystalline solid substrates are investigated using molecular-dynamics simulations for a range of molecule-to-solid interaction strengths, external loads, and film thicknesses. The confined films are infinite in extent in one of the directions parallel to the solid surfaces and finite in the other direction exposing a liquid-to-vacuum interface (i.e., semidroplet configuration). At sufficiently high loads, whose magnitude depends upon the molecule-to-surface interaction strength, layering, i.e., oscillations in the film density in the direction normal to the boundary, occurs accompanied by an enhancement of surface-parallel orientational ordering of the molecules in the interfacial region. In addition, preferential interfacial adsorption of chain ends, as well as molecular conformations enhancing bridging of the two solid surfaces, are observed. The dynamics of thinning, from a three- to a two-layer film, exhibits a marked dependence on the molecule-to-surface interaction strength. At a critical load the relatively strong adsorption system exhibits a sudden collapse to two layers, resulting in lateral stress accumulation, and subsequent spreading via a cooperative mechanism. On the other hand, thinning of the weakly adsorbed film is gradual, with no stress accumulation, accompanied by spreading occurring via diffusion and adsorption of molecules at the liquid-to-vacuum interface.

I. INTRODUCTION

Understanding the structural, dynamical, and rheological properties of fluids at interphase (solid-to-liquid and vapor-to-liquid) interfaces is of basic as well as practical importance, and studies of such systems have been the subject of a number of experimental and theoretical efforts. Such interfacial systems are ubiquitus in nature, occurring under equilibrium as well as nonequilibrium conditions (for example, liquid-phase epitaxy,[1] laser annealing,[2] surface melting,[3] liquid flow past solid boundaries, and shear flow of confined thin fluid films[4]), and are of relevance to diverse physical phenomena and technological issues, among them crystal growth, adhesion, wetting, film spreading and drainage, coating, droplet formation on solid surfaces, lubrication and wear, and stabilization of colloidal systems.[5]

Studies of such interfacial systems on the atomic or molecular scale pose significant experimental and theoretical challenges due to the very nature of the system, involving an interface between two many-body complex material phases. Furthermore, there is a body of experimental and theoretical evidence that confinement of a liquid between two solid surfaces or within any narrow confining space, whose dimensions are just a few molecular liquid diameters, affects in a very significant manner both the equilibrium and nonequilibrium structural and dynamical properties as well as response, rheological, and transport characteristics of the confined liquid.[5(a),5(b),6-9] This implies that concepts and treatments which are appropriate for investigations of bulk liquids have to be reexamined and reformulated to take explicit account of the new boundary conditions, interactions at the solid-liquid interface, and other factors which may characterize confined fluids.[9]

The combined fundamental and technological interest in the equilibrium and dynamical properties of confined fluids resulted in experimental and theoretical research endeavors aimed at enhancing our understanding of these systems with increasing spatial and temporal resolution. On the experimental front the advent and proliferation of proximal probes (the surface-force apparatus (SFA),[6,7,10] atomic-force microscopy (AFM),[11,12] and microbalance techniques[13]), open new avenues for measurements of interphase interfacial properties with refined (molecular) spatial resolution. On the theoretical front, several treatments (based on liquid-state perturbation theory and density-functional descriptions) have been applied to study model simple fluid equilibrium systems,[14-17] and statistical-mechanical theories of the thermodynamics and structure,[9,18(a),18(b)] as well as theoretical treatments of the dynamics[18(c)] of interfacial polymer systems have been developed. Alternatively, numerical approaches via molecular-dynamics (MD) and Monte Carlo (MC) simulations[19] alleviate certain difficulties which hamper analytical treatments (such as lack of symmetry, complex interactions and molecular structures, and large deviations from equilibrium) and allow direct interrogation of such systems with atomic-scale spatial and temporal (using MD) resolution. Early MD studies of interfacial systems employed model monoatomic liquids,[1,2,8,17,20-27] revealing interfacial liquid density ordering and variations in transport and dynamical properties of the liquid as a function of distance from the interface. In more recent investigations,[28-30] MD (and MC) simulations

were extended to studies of complex fluids demonstrating the marked effect of stationary constraining (impenetrable and structureless) solid boundaries on the properties of complex molecular liquids.

In this paper we investigate, using large-scale MD simulations, the properties of *n*-hexadecane ($C_{16}H_{34}$) films confined between two stationary, atomically structured crystalline solid boundaries in a configuration which allows us to investigate the structural and dynamical response of the film to variation in the external force applied normal to the confining solid surfaces. In our study the liquid film is confined in the normal direction (z) to the surface plane of the solid boundaries (xy plane). The film is extended via a periodic boundary condition in the x direction parallel to the surface plane and is finite in the other surface-parallel direction (y). Choosing this particular film configuration (semidroplet) rather than a continuous film of infinite extent in both directions parallel to the solid boundaries as in other investigations, allows the film the freedom to spread freely (in the y direction) in response to the application of a normal load, which simulates to a certain extent the conditions in the surface-force apparatus experiments[6,7,10,31] (simulations where large solid tips interact with liquid films or liquid droplets supported on solid substrates are in progress in our laboratory[32]). The computational methodology is described in Sec. II.

Results for structural, energetic, and dynamic properties of hexadecane films confined between two crystalline boundaries are given in Sec. III. The dependencies of the molecular distributions, conformations, orientational order, and dynamics of film thickness variations, in response to applied load normal to the confining solid crystalline boundaries are discussed for systems exhibiting weak and enhanced surface adsorption tendencies.

A summary of our findings is given in Sec. IV.

II. COMPUTATIONAL METHOD

In our simulations the hexadecane molecules are described by the interaction potentials developed by Ryckaert and Bellemans,[33] which have been demonstrated to provide an adequate description of bulk liquid properties.[33] In addition, these model potentials have been recently used[34,35] in studies of the rheological properties of bulk liquid *n*-alkanes yielding results (for zero shear rate viscosities) in agreement with experimental data. In this model the CH_2 and CH_3 groups are represented by a pseudoatom of mass 2.41×10^{-23} g, and the intramolecular bond lengths are fixed at 1.53 Å and the bond angles fixed at 109° 28'. A 6–12 Lennard-Jones (LJ) potential (where α and β refer to the identity of the interacting species),

$$\Phi_{\alpha\beta}(r) = 4\epsilon_{\alpha\beta}\left[\left(\frac{\sigma_{\alpha\beta}}{r}\right)^{12} - \left(\frac{\sigma_{\alpha\beta}}{r}\right)^6\right], \tag{1}$$

describes the intermolecular interaction between sites in different molecules, and the intramolecular interactions between sites more than three apart. An angle-dependent dihedral potential $\phi_D(\alpha)$ is used to model the effect of missing hydrogen atoms on the molecular conformation, with the parameters the same as those used in Ref. 33.

In the model which we use in our study the LJ interaction parameters (ϵ and σ) are the same for two sites (pseudoatoms) located, more than three apart, on the same molecule (i.e., intramolecular) or on different molecules (i.e., intermolecular). The values of these interaction parameters are $\epsilon_2 \equiv \epsilon_{ij} = 72$ K and $\sigma_2 \equiv \sigma_{ij} = 3.923$ Å, where $i \neq j$ correspond to molecular sites. The 6–12 LJ potential is truncated at $2.5\sigma_2$, and the constraints on intramolecular bonds and bond angles are treated via a recently proposed algorithm.[35(b)] The equations of motion were integrated using Gear's fifth-order predictor–corrector algorithm[19] with a time step $\Delta t = 0.002\tau$, where the time unit $\tau = 1.93$ ps. As a test we simulated bulk *n*-decane at a temperature $T = 481$ K and density $\rho = 0.630$ g/ml obtaining energetic and structural properties in agreement with previously published results.

It is appropriate at this point to reiterate that in our simulations the hexadecane molecules are modeled with both the bond lengths and bond angles constrained [with torsions represented via the dihedral potential $\phi_D(\alpha)$ as described above[33]]. The technical and physical issues related to constrained calculations have been discussed extensively.[19,36,37] While the consequences of constraints (especially fixing the bond angles) on equilibrium conformational properties (particularly gauche/*trans* populations) have been evaluated rather thoroughly,[19,36,37] their implication for dynamics are far more difficult to assess.[36,37(c)]

In this context it is of interest to note that in recent studies performed in our laboratory,[38] of the properties of adsorbed hexadecane liquid films of variable thickness (where the same constrained molecular model potentials were used), we have found that for the first adsorbed layer of a ~40 Å thick film, at 350 K, the percentages of *trans* (t) and gauche conformations (g_+ and g_-) are 79, 10.7, and 10.3, respectively, while in the middle region of the film (of near bulk density), $(t, g_+, g_-) = (66, 17, 17)$. The trend of the influence of the surface adsorption potential causing a higher percentage of *trans* conformations in the proximity of the solid–liquid interface then in the bulk is the same as that found in recent simulations[39] of *n*-decane adsorbed on graphite at 291 K, using the same 6–12 LJ and dihedral potentials, but with unrestricted bond angles (which were modeled using a harmonic potential[39]). Moreover, the conformational populations obtained in our simulation[38] compare favorably with those obtained from simple Boltzmann statistics, and other simulations.

On the basis of the above results, and because of the strong influence of the confining surfaces on the conformational and dynamical properties of the molecular film in our study, we do not expect a strong sensitivity of our results on the constrained molecular model (and the corresponding constrained class of motions) which we have used. Nevertheless, to alleviate this issue we plan to include bond-angle bending in future simulations.

The solid boundaries consist each of $n_{st} = 3$ layers of static atoms stacked as a face-centered-cubic (fcc) crystal exposing the close-packed (111) plane, with the z axis in the

direction normal to the surface. The system is periodically replicated in the x and y directions. [In test simulations we found that treating the surface atoms as dynamic particles at the temperature of our studies ($T = 6.68\epsilon_2 = 481$ K) has only a small effect on our results.] We note that the thickness of the solid boundaries is chosen to be larger than the range of the interaction potential between the molecules and the solid atoms (see below) and thus the molecular film can be considered as dynamically evolving between two confining semi-infinite crystalline boundaries. The solid boundaries were chosen to mimic a typical metal substrate (e.g., Ni), with the corresponding interatomic 6–12 LJ parameters $\sigma_{ij} \equiv \sigma_3 = 2.22$ Å (i.e., $\sigma_3 = 0.566\sigma_2$) and $\epsilon_{ij} = 6030$ K, where i and j refer to atoms in the solid boundaries. The interaction between a molecular site (pseudoatom) and a surface atom is described also by a 6–12 LJ potential with $\sigma_{\alpha 3} = 0.566\sigma_2$, where α denotes a molecular site (pseudoatom) and 3 an atom in the solid boundary, and with two values for $\epsilon_{\alpha 3} \equiv \epsilon_3$, one corresponding to the molecule–solid interactions being equal to those of intra- and intermolecular one (i.e., $\epsilon_3 = \epsilon_2$), and the other where it is three times stronger (i.e., $\epsilon_3 = 3\epsilon_2$), simulating the case of enhanced tendency of molecular adsorption. (Here and in the rest of the paper results are given in units of σ_2, ϵ_2, and τ.) Since precise values of interatomic interaction strength between n-alkanes and material substrates are not accurately known, the above values encompass a range of possible values.[40] Indeed, our simulations demonstrate systematic dependence on the strength of the molecule-to-substrate interaction.

The n-hexadecane semidroplet is set up to extend over the whole computational cell in the periodically replicated direction (x), and is finite (exposing liquid to vapor, or vacuum, interfaces) in the y direction. The dimension in the y direction (L_y) is of sufficient size that a molecule at the center of the droplet will not directly experience the influence of the vacuum/fluid interface, i.e.,

$$L_y/2 > r_{max} + r_c. \tag{2}$$

Thus the semidroplet has, to some extent, both an interior region and a liquid–vapor interface. The x dimension is also chosen so that no molecule can interact with its own periodic image. Here r_{max} is the largest end-to-end extension of a molecule (i.e., when the molecule is stretched in an all-*trans* configuration), and $r_c = 2.5\sigma_2$ is the cutoff distance for the LJ potential. We selected this semidroplet configuration so that in future studies we could maintain steady state (in the x direction) for any shear rate without having to worry about artifacts due to the finite size of the droplet. Furthermore, we chose the y cell dimension L_y to be large enough that a molecule could detach from the semidroplet and displace far enough in the y direction so that it completely lost contact with the droplet, before it encounters the cell boundary. This property is important since molecules will occasionally detach from the semidroplet as we increase the load in the z direction; when they wander far enough, we can merely remove them from the simulation without affecting the semidroplet dynamics.

To satisfy the above conditions and to allow sufficient space in the y direction so that the droplet can spread, or even lose molecules, without encountering the cell boundary, we chose each static solid slab to have xy dimensions accommodating 15×210 particles per solid layer. The hexadecane semidroplet occupies throughout our simulations the entire extent of the substrate in the x direction and only a portion of it in the y direction, and it contained 115 hexadecane molecules (i.e., 1840 pseudoatoms).

While in simulations where the solid substrate atoms are treated dynamically the temperature is controlled via scaling of the velocities of solid particles, in simulations where the crystalline solid is treated statically (as in this study) temperature is controlled via velocity scaling of the molecular film at infrequent times during the simulations. We have verified that the temperature control in our simulations (which establishes a constant-temperature, macrocanonical ensemble) does not affect in any discernable way the results of our studies.

Finally, we may investigate our systems in two modes: (i) a constant-thickness mode where the average internal stresses may vary, and (ii) a constant-load mode where, at steady state, the average internal uniaxial stress in the direction of the load is constant (and equal to the external load), and the thickness of the system varies dynamically. In both modes shear can be induced by moving the solid slabs at a fixed velocity with respect to one another. In this paper we present only results for the constant-load mode. In this mode we apply an external force

$$F_{ext} = \tau_{zz} A_s, \tag{3}$$

to the exposed surfaces of the static slabs where τ_{zz} is the external normal load (the only nonzero component of the external stress tensor) and A_s is the area of the solid substrate. It should be noted, however, that the *load on the semidroplet itself* is *different* from that given in Eq. (3) since the *real area of contact* between the liquid semidroplet film and the substrate (see A_c in Table I) is not given by A_s, and in addition it may vary in response to the applied external force. (In terms of the energy and length units which we use, ϵ_2 and σ_2, the unit of force is 1.868×10^{-2} N and that of load, or pressure, is 12.138 MPa, where 1 Pa = 1 N/m^2.) These considerations are discussed further in Sec. III.

III. RESULTS

A. Equilibration

The molecular complexity of the n-alkane liquids dictates special care in ensuring proper equilibration of the system, to avoid inadequate exploration of the accessible phase space due to the complicated nature of the configurational space.

Our initial setup of the simulations was the same for both systems (i.e., $\epsilon_3 = \epsilon_2$ and $\epsilon_3 = 3\epsilon_2$). We initially equilibrated each system with the hexadecane molecules spread uniformly across a slab with xy dimensions of 15×50 static particles. The molecules were initially lined up flat (all in a *trans* conformation) in rows in several layers. The sys-

TABLE I. External applied load (L_{ext}), internal load (L_{int}), film thickness in the normal direction to the solid boundaries (d_z), extent of the film along the y direction parallel to the solid surfaces (d_y), i.e., full width at half maximum of the segment (pseudoatom) density profile in the y direction between the two liquid-to-vacuum interfaces (see, e.g., Fig. 1), and area of contact (A_c) of the film (calculated using d_y and the extent of the film in the x direction). The total area of the solid surface is $1060\sigma_2^2$. L_{int} was calculated by averaging all forces on surface atoms due to molecules in an area well within the middle region, and then dividing the average force by that area. d_z was calculated by subtracting σ_2 from the distance between the opposing proximal solid surfaces measured with respect to the centers of the atoms in these layers. The time spans of the simulations for the different values of applied load are given by τ (in ps). Loads in units of $\epsilon_2/\sigma_2^3 = 12.138$ MPa, length in units of $\sigma_2 = 3.923$ Å, and area in units of $\sigma_2^2 = 12.92$ Å^2.

L_{ext} (ϵ_2/σ_2^3)	L_{int} (ϵ_2/σ_2^3)	d_z (σ_2)	d_y (σ_2)	A_c (σ_2^2)	τ (ps)
		$\epsilon_3 = \epsilon_2$			
0.1	0.43	6.6	21.6	174.7	386
0.3	1.27	4.5	31.3	253.2	386
0.5	1.63	3.6	37.6	304.1	386
0.9	2.38	2.9	45.0	374.0	772
1.0	2.36	2.2	60.5	489.4	772
		$\epsilon_3 = 3\epsilon_2$			
0.1	0.47	2.94	40.2	325.2	386
0.4	1.55	2.88	40.7	329.2	772
0.5	1.48	1.81	61.3	495.8	656

FIG. 1. Density profile of the pseudoatoms (segments) of the n-hexadecane molecules vs y (the direction parallel to the confining solid surface planes, exposing liquid-to-vacuum interfaces of the semidroplet) for a system characterized by $\epsilon_3 = 3\epsilon_2$, i.e., strong adsorption, and $L_{ext} = 0.5$ (see Table I). The distance between the down arrows corresponds to the internal region of the film in the y direction and the up arrows indicate the full width at half maximum of the alkane system. Density in units of σ_2^{-3} and length in units of $\sigma_2 = 3.923$ Å. To convert the number-density profile to mass density in g/cm^3 multiply by 0.398.

tem was allowed to evolve for a long time at a temperature $T = 6.68$ (481 K) with an external load $\tau_{zz} = 1.5$ (in previous calculations we observed that under these conditions our alkane system had a density close to that used in several other calculations). To thoroughly "mix" our system we undertook the following procedure. After initial equilibration we turned off the attractive part of the liquid-to-solid interaction and raised the temperature to $T = 12$. The dynamical slab immediately expanded to twice or more times its original thickness, and three-dimensional snapshots of the alkane structure, taken after about $40\,000\Delta t$, revealed that the system had lost its initial interfacial structure and the molecules were thoroughly mixed. After the distance between the two solid boundaries had stopped increasing and the system was allowed to evolve, we turned on the attractive part of the liquid-to-solid interaction and lowered the temperature to $T = 6.68$. Subsequently, we equilibrated the system (typically for $40\,000\Delta t = 155$ ps) and then transferred the positions of the alkane molecules in the calculational cell to the middle of a slab with the same dimension in the x direction but with an extended length of 210 atomic rows in the y direction. The preparation stage was then completed following another period (155 ps) of equilibration.

B. Structural results

Having equilibrated the systems as described above we have studied the properties of the n-hexadecane semidroplet under various applied loads. For each load the system was equilibrated for an extended period (see Table I) and average properties were calculated after equilibrium had been achieved (i.e., when no discernable trends are observed in energetic and structural properties beyond natural fluctu-
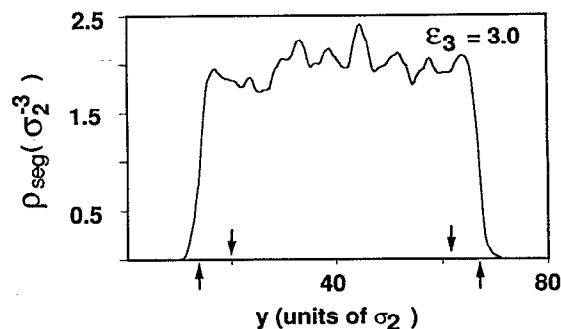
ations). In all cases statistical averages were performed over $40\,000\Delta t = 155$ ps following equilibration.

Before discussing the film properties along the direction normal to the solid boundaries we show in Fig. 1 a pseudoatom (sometime called segment) time-averaged density profile along the y direction, for the system with $\epsilon_3 = 3\epsilon_2$ (i.e., characterized by a relatively strong adsorption tendency of the hexadecane molecules to the solid substrate) and for a relatively high external load of 0.5 (see Table I; as discussed below for this value of the load the film may be characterized as consisting of two layers in the normal, z, direction). As seen, the system consists of an internal liquid region and liquid-to-vacuum interfaces characterized by sharp drops of the liquid density (the full width at half maximum locations are marked by up arrows on the y axis).

The concave shape of the meniscus (film edge) at the liquid-to-vacuum interface for the system shown in Fig. 1 is evident from Fig. 2(B) where we show the average locations of edge pseudoatoms (marked by $\times$'s), in slices along the film thickness (z direction) as a function of y. For comparison a profile for the system characterized by weak adsorption to the substrate (i.e., $\epsilon_3 = 1\epsilon_2$) and for an external load of 0.1 (when the film thickness is $\sim 6\sigma_2$), exhibiting a convex meniscus, is shown in Fig. 2(A). The difference in curvature of the meniscus of the confined semidroplet at the liquid-to-vacuum interface reflects the different molecule-to-substrate interactions for the two systems, and is the subject of a separate study.

For the purpose of most of the studies presented herein we focus on properties of the liquid film within the wide region not including the liquid-to-vacuum interface. Consequently, in presenting our results properties are averaged for molecules located in the internal region of the semidroplet along the y direction (marked by down arrows in Fig. 1) defined as the region internal to the outmost density peak in the density profiles, $\rho_{seg}(y)$.
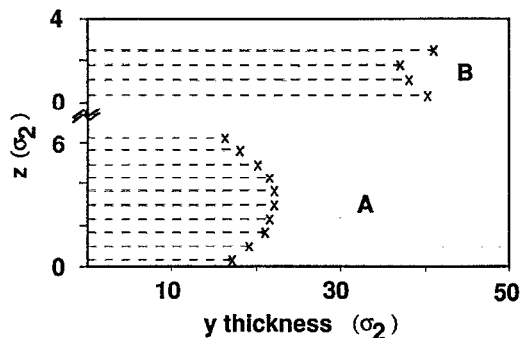
Profiles of the segment density (i.e., pseudoatom distri-

FIG. 2. Shape of the miniscus (film edge) formed at the liquid-to-vacuum interface of n-hexadecane films for the system characterized by weak adsorption to the solid substrate ($\epsilon_3 = \epsilon_2$) with $L_{ext} = 0.1$ (see Table I) and for the one with $\epsilon_3 = 3\epsilon_2$ and $L_{ext} = 0.5$ (see Fig. 1). $\times$'s denote the average y location of edge pseudoatoms averaged in slices through the film along the z direction (dashed lines, along the y axis are drawn to guide the eye). Distances in units of $\sigma_2 = 3.923$ Å.

FIG. 4. Same as Fig. 3, but for a system characterized by strong interaction between the n-hexadecane molecules and the solid substrate ($\epsilon_3 = 3\epsilon_2$). A, B, and C correspond to systems with $L_{ext} = 0.1, 0.4$, and 0.5, respectively. Curves B and C are shifted upwards by four units along the ordinate axis, for clarity.

bution), along the direction normal to the solid interfaces $[\rho_{seg}(z)]$, for the two systems ($\epsilon_3 = \epsilon_2$ and $\epsilon_3 = 3\epsilon_2$), and for various external, and correspondingly internal loads (see Table I) are shown in Figs. 3 and 4, respectively. (The origin of the z axis is located at the center of the atoms in the proximal crystalline solid surface layer of one of the solids bounding the film.) The oscillatory character of the segment density profiles, which becomes more pronounced as the load is increased and the systems thin correspondingly (see also Table I), is evident. In addition, the magnitude of the density oscillations is larger for the $\epsilon_3 = 3\epsilon_2$ system, which is markedly thinner (compare Figs. 3 and 4, and d_z values in Table I, for $\epsilon_3 = \epsilon_2$ and $\epsilon_3 = 3\epsilon_2$) for equivalent external loads, due to the increased attraction between the molecules and the solid boundaries. Furthermore, we note that the pe-
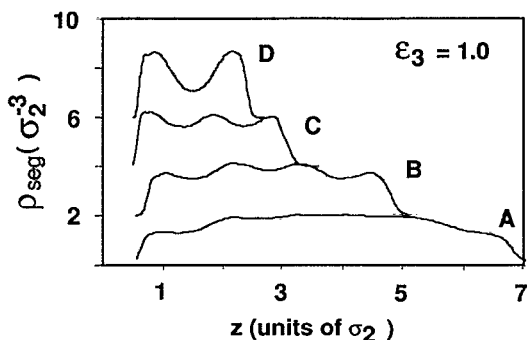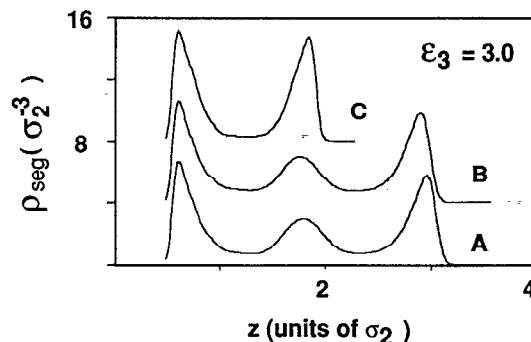
riodicity of the oscillations for a given value of ϵ_3 is only mildly dependent on load [compare Figs. 3(a)–3(d), and Figs. 4(a)–4(c)], and its value ($\sim 1\sigma_2$, i.e. ~ 4 Å), which is comparable to the value obtained via surface-force measurements[7(a),31] is similar for both interaction strengths (compare Figs. 3 and 4), with that for $\epsilon_3 = 3\epsilon_2$ smaller by about 10%–20%. We do observe, however, that the peak of the first (closest to the solid boundary) density oscillation for the weakly adsorbed molecular system (i.e., $\epsilon_3 = \epsilon_2$) occurs at a larger distance from the solid boundary than its location for $\epsilon_3 = 3\epsilon_2$, reflecting the enhanced attraction between the molecules and the solid in the latter case.

It is interesting to note that for the weak adsorption system, even for the three-layer film [Figs. 3(A)–3(C)], the density in the layers (~ 0.79 g/cm^3) is similar to that of bulk hexadecane. For the strong adsorption case the density in the layers close to the solid boundaries is much higher than bulk density and for the two lower load values [Figs. 4(A) and 4(B)] the middle-layer density is below that of the bulk.

Prior to discussing further the density oscillations and their origins we turn first to other results pertaining to conformational properties of the film molecules (figures of those quantities described below and not included in the paper are available upon request from the authors). Profiles of the gyration radii (R_g) of the hexadecane molecule, and their components (R_g^α, where $\alpha = x,y,z$), for the two values of the molecule-to-surface interaction (ϵ_3) and in each case for several values of the external load (and correspondingly film thickness), plotted as a function of the distance of the center of mass of the molecules from the solid interface, reveal that the values of the radii of gyration are similar for the two ϵ_3 values, and in each case they show a slight decrease as the load is increased (i.e., thinner films). Furthermore, R_g is of the order of $\sim 1.15\sigma_2$, i.e., a little larger than the "width" of the hydrocarbon chain (σ_2). Second, in both cases molecules whose center of mass (CM) is located closer to the solid interface are characterized by a somewhat larger value of R_g than those whose CM is further away. Moreover, the normal components of the gyration radii (R_g^z) exhibit a strong dependence on the molecular CM distance from the interface, reflecting a strong distance-dependent molecular

FIG. 3. Segment (pseudoatom) density profiles vs z (i.e., in the direction normal to the solid surfaces with the origin at the center of the atoms belonging to the solid surface layer, closest to the molecular film, in one of the confining crystalline boundaries) for n-hexadecane interacting weakly with the solid ($\epsilon_3 = 1\epsilon_2$). Results are shown for four values of the external load $L_{ext} = 0.1, 0.3, 0.9$, and 1.0 marked by A, B, C, and D, respectively. The depletion in the pseudoatom density near the solid boundary for the lowest load (A) and the density oscillations for higher load, and correspondingly thinner films, are noted. Density in units of σ_2^{-3} and distance in units of $\sigma_2 = 3.923$ Å. Curves B, C, and D are shifted upwards by two units along the ordinate axis, for clarity.

conformational anisotropy. We observed that for both ϵ_3 values and for the low external load values the three R_g^α components achieve similar values for molecules whose CM's are located toward the center of the liquid film. We note here that while for the weak-adsorption case ($\epsilon_3 = 1\epsilon_2$) the molecular film extends over a thickness $d_z = 6.6\sigma_2$ for the lowest applied load, d_z is only $2.94\sigma_2$ in the strong-adsorption case ($\epsilon_3 = 3\epsilon_2$). Consequently, a bulklike region in the film is not to be expected for any of our load values for the $\epsilon_3 = 3\epsilon_2$ case. It is of interest to remark that for the $\epsilon_3 = 1\epsilon_2$ case the components of the radii of gyration become isotropic at $\sim 2\sigma_2$, i.e., at $\sim 2R_g$, as has been noted previously in studies of other interfacial systems.[28,29] We further observe that for both systems under high loads and thus thin molecular films, the influence of the solid boundaries does not damp at the middle of the liquid film, which for small thickness ceases to have a bulklike region and is thus wholly interfacial in nature.

The marked anisotropy of the components of the radii of gyration, with $R_g^z < R_g^x$, R_g^y, in the interfacial region, implies that for a wide range of adsorption strengths the molecules in that region (or large portions of them consisting of several segments) tend to assume "flattened" conformational shapes whose dimensions parallel to the interface are larger than in the normal direction.

To further characterize the molecular conformations in the interfacial region we have analyzed the variation of orientational order parameters for our systems, as a function of distance from the solid boundaries. For both cases ($\epsilon_3 = 1.0$ and 3.0) we found that two-bond vectors (i.e., $r_{i,i+2}$ connecting pseudoatoms i, and $i + 2$, with $1 \leqslant i \leqslant 14$, in the same molecule) in the proximal interfacial region are preferentially aligned parallel to the interface, while in the bulklike region they are randomly oriented. Furthermore, for the weak-adsorption system the orientational alignment is found to be stronger for the thinner film and the tendency for parallel-bond orientation is enhanced for increased adsorption strength. It should be emphasized, however, that the two-bond preferential orientational anisotropy decays rapidly with distance away from the solid boundary, even for the thickest film (e.g., for a $\epsilon_3 = 1.0$ and external load of 0.1) preferential order vanishes at $z \sim 1.25\sigma_2$. (Considering that the origin was taken at the centers of the solid atoms in the perfectly crystalline layer closest to the molecular film the decay of the bond-orientation anisotropy is seen to occur over a distance of less than $1\sigma_2$ from the onset of the repulsive interaction between the pseudoatoms in the molecules and the surface atoms.) We also note that for the strong-adsorption case and for small load that the two-bond order parameter oscillates, assuming negative values in regions corresponding to density maxima (see, e.g., curve A in Fig. 4). This indicates that better packing in the film layers is obtained via preferential alignment of two-bond vectors parallel to the solid boundaries [similar to the results in Ref. 28(a)].

Further analysis shows that the preferential alignment of the planes of the two-bond segments is weaker than that found for the two-bond vectors, and decays faster as a function of distance from the solid boundary. In fact, our results indicate that while in the region of the film in very close proximity to the solid boundary a tendency for parallel-to-the-wall orientation is apparent, two-bond segments located in the first interfacial layer are preferentially oriented with their planes parallel to the z axis, i.e., normal to the solid boundaries (while as aforementioned the corresponding two-bond vectors are preferentially oriented parallel to the solid surface).

Additional conformational information is obtained from distributions of molecular end-to-end distances, R_{end} (the distance from pseudoatom 1 to the end pseudoatom, 16) plotted vs the distance of the molecular CM from the solid boundary. From such distributions we observe that in all cases the R_{end} distance is smaller than the fully extended length (all-*trans* configuration) of the hexadecane molecule [$(16–1)\,0.637\sigma_2/2 = 4.78\sigma_2$]. Overall, the characteristics of the curves are similar to those deduced for the molecular radius of gyration with R_{end} for molecules in the interfacial region larger ($\sim 3.4\sigma_2$ and $3.7\sigma_2$ for the weak- and strong-adsorption cases, respectively), than for those further away from the solid boundary ($\sim 2.7\sigma_2$ and $3\sigma_2$ for the two-adsorption strength, respectively), correlating with the molecular preferential parallel orientation near the solid interfaces.

Having discussed certain conformational properties of the molecules and their dependence on adsorption strength and external load (and thus film thickness) we return now to issues related to the distribution of the molecules in the confined film. In Figs. 5(b) and 6(b) we show for the two-adsorption strength and for a series of external loads, profiles of the distribution of center-of-mass locations [$\rho_{mol}(z)$] with reference to their distance from the solid boundaries.
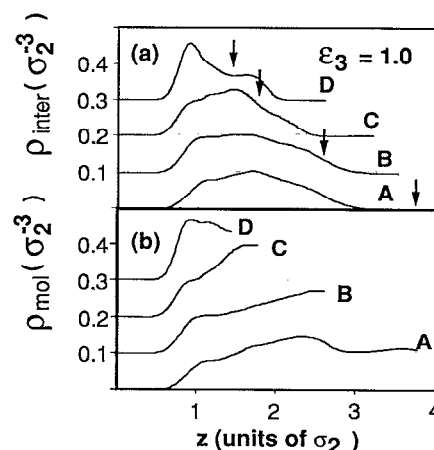

FIG. 5. Profiles of center-of-mass location vs distance from the solid surface, ρ_{mol} [in (b)], and of the center-of-mass location for molecules having at least one of their pseudoatoms in the interfacial region of width $\Delta z_{inter} = 1.1\sigma_2$ from the solid surface [ρ_{inter}, in (a)]. The origin of the z axis is located at the center of atoms in the proximal solid surface layer. Results are given for the system characterized by $\epsilon_3 = 1\epsilon_2$, and for $L_{ext} = 0.1, 0.3, 0.9$, and 1.0 denoted as A, B, C, and D, respectively. Down arrows mark the center of the film. The results are averaged over the two interfaces. Curves B, C, and D are shifted by 0.1 upwards, for clarity. Density in units of σ_2^{-3} and length in units of $\sigma_2 = 3.923$ Å.
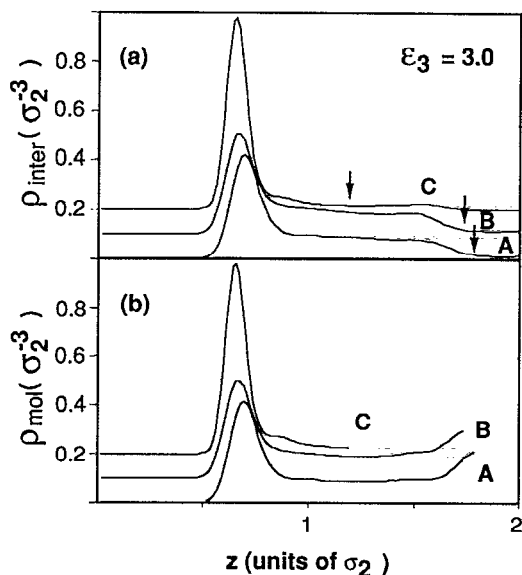
FIG. 6. Same as Fig. 5, but for the system characterized by $\epsilon_3 = 3\epsilon_2$, and with $\Delta z_{inter} = 1.0\sigma_2$. A, B, and C correspond to $L_{ext} = 0.1$, 0.4, and 0.5, respectively.

As seen, in all cases the first peak [better characterized as a shoulder for curves A–C in Fig. 5(b)] occurs at $\sim 1\sigma_2$, and is further removed from the interface than the location of the first maximum in the corresponding pseudoatom (or segmental) density profiles shown in Figs. 3 and 4. This is a manifestation of the fact that the molecules in the interfacial region are not lying all flat parallel to the interface. In fact, for the weak-adsorption case we find that the highest value of ρ_{mol} is attained toward the middle of the film [compare Fig. 5(b) and Fig. 3]. Note, however, that for the lowest load, shown as case A in Fig. 5(b) (i.e., a film of thickness $d_z \sim 6.6\sigma_2$; see Table I), ρ_{mol} in the bulklike region near the middle of the film decreases somewhat after achieving a maximum value at $z \simeq 2.3\sigma_2$. We also observe that the location of the first maximum in ρ_{mol} shifts somewhat to a smaller distance from the solid boundary as the load is increased.

For the strong-adsorption case shown in Fig. 6(b) the molecular center-of-mass profile exhibits for the three external loads a single maximum at a distance significantly smaller than the radius of gyration of the molecules reflecting the tendency of large portions of molecules to adhere to the solid boundary and consequently the pronounced anisotropy of the molecular shape.

Profiles of the distribution of molecular center of mass for molecules having *at least one* of the pseudoatoms in a region of width Δz_{inter} from the solid boundary are shown in Figs. 5(a) and 6(a) (the magnitude of Δz_{inter}, $1.1\sigma_2$ for the system with $\epsilon_3 = \epsilon_1$ and $1.0\sigma_2$ for the strong-adsorption case $\epsilon_3 = 3\epsilon_2$, is chosen to be comparable to the average radius of gyration of the molecules, which approximately is also the width of the first layer in the film (see ρ_{seg} in Figs. 3 and 4). (In these plots the middle of the film thickness, for each value of the load, is denoted by an arrow.) These results corroborate our earlier conclusions pertaining to the observation that even though a portion of a molecule may be local-

ized in the proximity of one of the solid boundaries other segments of the molecule maintain a degree of conformational freedom and thus may be found in regions further away from the interface. Moreover, our results show that when the distance between the solid boundaries is small enough (i.e., thin molecular films) molecules may have parts of them adsorbed at one of the solid boundaries and parts near the middle of the film or close to the other boundary, i.e., molecules which tend to bridge the two confining interfaces [see, in particular, Fig. 5(a), curve D, where the shoulder, extending to the right of the arrow, indicating the midpoint distance between the solid boundaries, corresponds to molecules which have at least one segment adsorbed at one of the boundaries but their centers of mass located closer to the other boundary].

In previous studies preferential adsorption of chain ends to solid (structureless) surface has been observed[28,29] and it has been argued that entropically the presence of the solid surface excludes a larger number of chain configurations with middle segments in the proximal interfacial region than configurations with end segments adsorbed at the surface. Analysis of fractional segment occupancies, $f_s(z)$, expressing the probability for segment s of a molecule to be located in a region about z,[28(a)] shows for our systems a marked tendency of the molecular chain ends (pseudoatoms 1 and/or 16) to be localized at the interfacial region proximal to the solid boundaries, while other segments, corresponding to pseudoatoms 2 and/or 15, 3 and/or 14, etc., are located both in this proximal region as well as in regions of the film further removed from the solid surfaces. For the thickest film in the weak-adsorption case a tendency for successive pseudoatoms (starting from the chain ends and moving towards the middle ones) to occupy regions successively closer to the middle of the film is observed. This tendency remains for thinner films. For the strong-adsorption case the above trends are much less pronounced. Our results suggest that for thin molecular films interacting sufficiently strongly with a solid surface, the energetics becomes the dominant factor determining the interfacial molecular conformations.

Further information about the molecular conformations was obtained via study of the *conditional* fractional segment occupancy distributions $f_s^{s'}(z)$ which are defined in a manner similar to $f_s(z)$, but conditioned on pseudoatom s' of the molecule being located in the proximal interfacial region, Δz_{inter} (see Appendix A).

For the weak adsorption system ($\epsilon_3 = 1\epsilon_2$) we observe that for a thick film conformations where both ends are attached to the same solid boundary are common. Moreover, a large fraction of the molecules have one of their ends attached to one of the substrates and the other end located further from it toward the middle of the film. We also observe that for molecules which are attached to a substrate via their middle segments the end segments tend to be located further away from that boundary. Thus, for the thick weakly adsorbed film, interfacial molecules exhibit two main classes of conformations; the dominant class involves molecules where one or both chain ends are adsorbed at the interface (the chain-end enhancement mentioned above). Those molecules where both chain ends are adsorbed at the same inter-

face may be described as "end stapled molecules." The other main conformational class involves molecules attached to one of the solid surfaces via their middle segments and the chain ends are free (i.e., extending away from that solid surface toward the middle of the film). This situation remains true for a much thinner film (i.e., two-layers) although for this case the probability for molecular configurations with both chain ends as well as the middle stapled is higher.

The strong-adsorption system, for which at the low load the system is characterized as a three-layer system (see Fig. 4, curve A), also exhibits stapled configuration, with a larger tendency for both ends of a molecule as well as its middle segments to be attached to the same surface. The occurrence of such configurations is even larger for the two-layer film.

In closing this section we remark that in addition to the molecular conformations discussed above, a small fraction of the molecules are found in conformations which tend to bridge the two confining solid surfaces. Such bridging configurations occur for film thicknesses comparable or smaller than the length of the fully extended molecules (i.e., about $5\sigma_2$). We observed that bridging is more prevalent for the weakly adsorbed system [see Fig. 5(a)] although it is also

found in the strongly adsorbed case (see Fig. 9). Such bridging conformations have been suggested in the context of surface-force measurements where enhanced attraction between mica surfaces across hydrocarbon liquids, far exceeding the Van der Waals attraction predicted by the Lifshitz theory, has been observed.[41]

C. Dynamics of thin-film thickness transitions

Our discussion to this point centered on equilibrium structural properties of the confined *n*-hexadecane molecules for various external loads and corresponding film thicknesses. In this subsection we briefly discuss the dynamical characteristics of the film in response to applied load (a comprehensive study of this subject will follow).

For the two- adsorption strengths ($\epsilon_3 = \epsilon_2$ and $\epsilon_3 = 3\epsilon_2$) we focus on the dynamics of the transition from films characterized initially by a thickness $d_z \simeq 2.9\sigma_2$ [i.e., three-layer films with a thickness of about $3R_g$; see Fig. 3(C) and Fig. 4(D)] to two-layer films [see Figs. 3(D) and 4(C)]. The time evolution of d_z, the FWHM of the film in the *y* direction d_y (see e.g., Fig. 1), the pairwise contribution to the potential energy of the molecules, E_{p2} (i.e., the potential energy excluding the dihedral potential contribution, E_D) and E_D, are shown in Figs. 7 and 8, for the two mole-
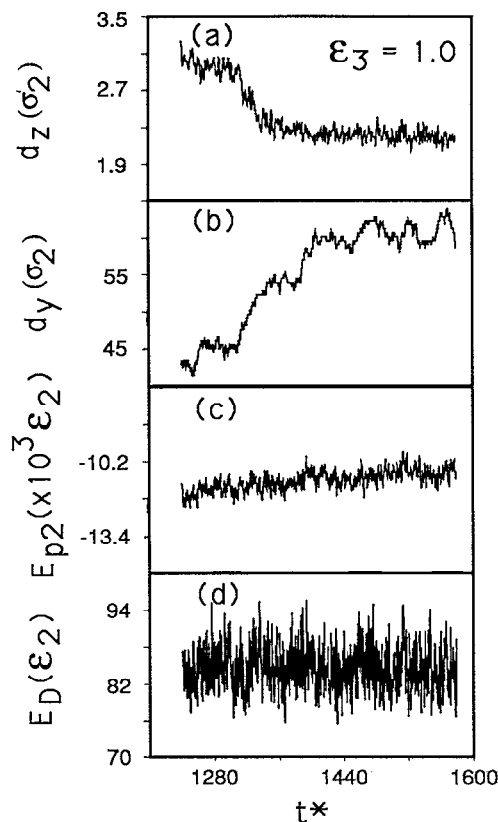

FIG. 7. Time evolution of the film thickness (d_z), the full width at half maximum of the film in the *y* direction (d_y), pairwise contribution to the potential energy of the molecules (E_{p2}), and dihedral potential contribution (E_D), plotted vs time t^* (in units of $\tau = 1.93$ ps). The time evolution starts upon incrementing the external load from $L_{ext} = 0.9$ to 1.0 (see Table I), for the system characterized by $\epsilon_3 = 1\epsilon_2$. Note the gradual variation in thickness (d_z) accompanied by spreading of the film (d_y).
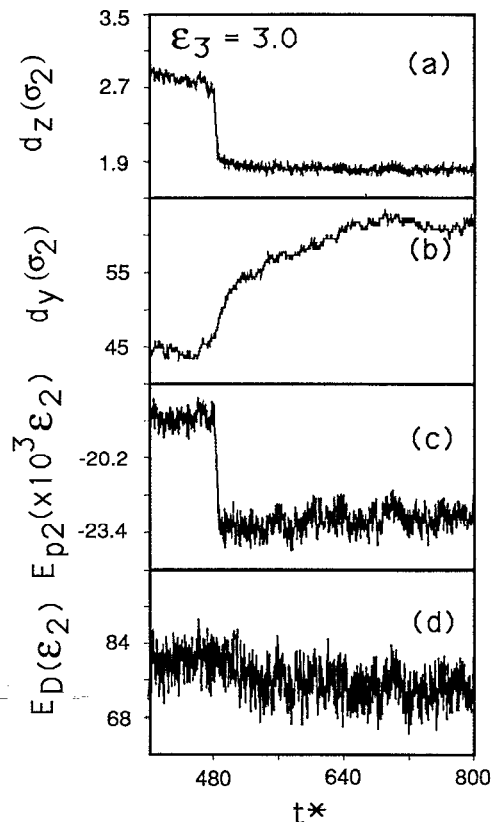

FIG. 8. Same as Fig. 7, but for the system characterized by $\epsilon_3 = 3\epsilon_2$, starting from the time that the external load was incremented from $L_{ext} = 0.4$ to 0.5. Note the sudden change in film thickness [in (a)] and subsequent spreading of the film [in (b)].
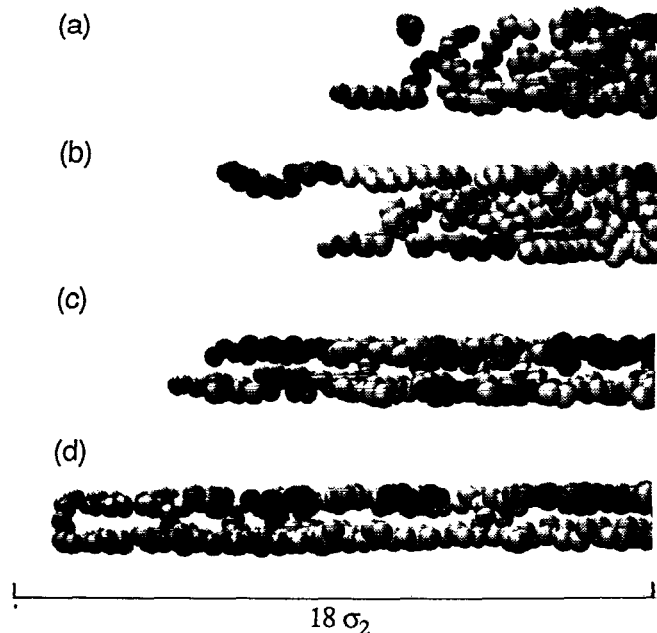
(a)

(b)

(c)

(d)

18 σ_2

FIG. 9. Snapshots of molecular configurations for the edge of the film characterized by $\epsilon_3 = 3\epsilon_2$ at selected times during its dynamical evolution (see Fig. 8). (a)–(d) correspond to $t^* = 400\tau, 475\tau, 520\tau$, and 700τ, respectively. The linear dimension (in the y direction) of the fraction of the system being shown is noted at the bottom of the figure. For all the snapshots the right-hand-side reference point on the y axis is the same.

FIG. 10. Diagonal components of the stress tensor for segments (pseudoatoms) in the interfacial region close to the solid substrate, vs time (t^*, in units of $\tau = 1.93$ ps) following increment of the external load from 0.4 to 0.5 at $t^* = 400$, for the system characterized by strong molecular adsorption ($\epsilon_3 = 3\epsilon_2$). Note the sudden increase in stress in (a) and (b) coinciding with the collapse of the film from three to two layers [see Fig. 8(a)], followed by relaxation. The interfacial region is defined here as one-third of the film thickness at any given time.

cule-to-surface interaction strengths, respectively. In both cases we start from an equilibrium stable three-layer system at the moment that the load is incremented (from an external load of 0.9 to 1.0 for $\epsilon_3 = 1$ at $t^* = 1240\tau$, and from 0.4 to 0.5 at $t^* = 400\tau$, $\tau = 1.93$ ps). As seen from inspection of the time evolution of d_z [Figs. 7(a) and 8(a)] both systems thin down in response to the added increment of the external load. However, the transition for the weak-adsorption system is relatively gradual involving only mild variations in the potential energies, while that for $\epsilon_3 = 3\epsilon_2$ is sudden, accompanied by a discontinuous large variation in E_{p2} [see Fig. 8(c)], and a relatively small decrease in the dihedral potential energy.

We also note that while for $\epsilon_3 = \epsilon_2$ spreading of the film [see d_y in Fig. 7(b)] coincides with thinning, for $\epsilon_3 = 3\epsilon_2$ most of the film spreading occurs subsequent to the abrupt change in thickness [see d_y in Fig. 8(b)]. Shown in Fig. 9 are snapshots of molecular configurations, near the film-to-vacuum interface (along the y direction, viewed from the side), for the $\epsilon_3 = 3\epsilon_2$ system, selected before ($t^* = 400\tau$), at the onset of the thickness transition ($t^* = 475\tau$) and after the transition ($t^* = 520\tau$ and 700τ), illustrating thinning and spreading of the film.

Video inspection of the time evolution reveals that in the case of strong molecule-to-surface interaction the transition from a three- to a two-layer film preceeds the spreading process. The film thinning in the first stage is achieved via packing of molecules in the proximal interfacial region and increased stress in the lateral directions (see Fig. 10). The dominant contribution to the stress peak is due to intermole-
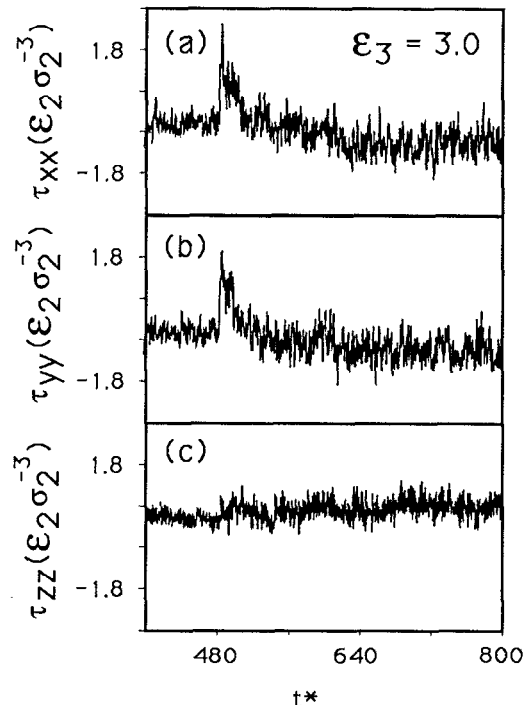
cular interactions. Upon achieving a critical density in this region, stress is relieved via a "cooperative diffusion" process. On the other hand, the thinning process of the system characterized by weak molecule-to-surface interactions ($\epsilon_3 = 1\epsilon_2$) does not involve stress accumulation (see Fig. 11) and is less cooperative in nature, involving drainage via diffusion and adsorption of molecules at the film-to-vacuum interface. The molecular mechanisms of drainage and surface wetting by complex liquids are of current interest,[42] and further studies in our laboratory of these phenomena are in progress.

IV. SUMMARY

We have investigated via molecular-dynamics simulations the structure and certain aspects of the dynamics of thin n-hexadecane films confined between parallel, atomically structured (i.e., crystalline), stationary solids in a configuration which allows the film to spread freely on the solid surfaces in one of the lateral directions (i.e., a semidroplet, or strip, configuration where the film is confined in the z direction normal to the xy planes of the solid boundaries, is extended in the x direction via periodic boundary conditions, and is of finite width in the y direction). In our simulations the molecular degrees of freedom (subject to bond-length and bond-angle constraints; see Sec. II) as well as the spacing between the confining solid boundaries evolve dynamically.
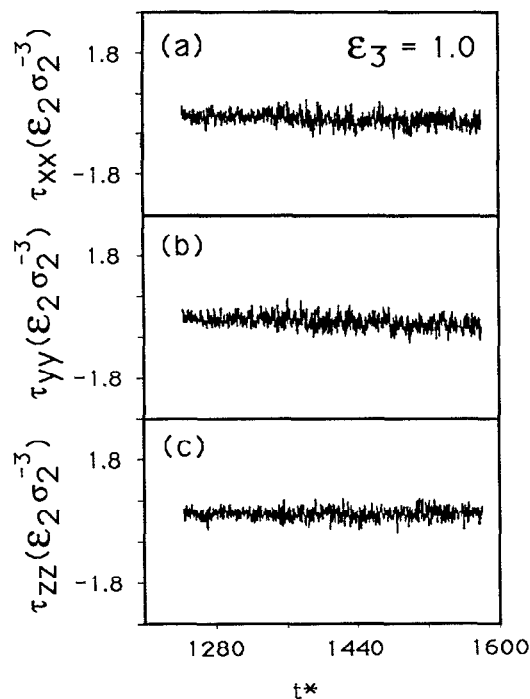
FIG. 11. Same as Fig. 10, for the weak-adsorption system (i.e., $\epsilon_3 = 1\epsilon_2$), starting upon incrementation of the external load from 0.9 to 1.0. Note, that in contrast to the $\epsilon_3 = 3\epsilon_2$ case (Fig. 10) no stress accumulation accompanies the film thinning process.

To investigate dependencies of the properties of the films on the strength of interaction between the film molecules and the solid substrates two sets of simulations were performed. In one of them (which we term weak adsorption) the interaction strength (denoted as ϵ_3) between a surface atom and a molecular CH_2 segment was assumed to be equal to the intra- or intermolecular interaction (ϵ_2) between two (CH_2) segments (i.e., $\epsilon_3 = \epsilon_2$), and in the second case (which we term strong adsorption) an enhanced surface adsorption strength is assumed (i.e., $\epsilon_3 = 3\epsilon_2$). (This value corresponds to a surface adsorption energy per CH_2 segment comparable to that obtained from thermal desorption measurements for alkanes on a variety of metal surfaces, i.e., ~ 1 kcal/mol per CH_2 segment.[40])

Starting for low values of the external loads from an unstructured segment density profile of the film (along the film thickness, i.e., z direction), the thickness of the film decreases and its lateral extent increases (see d_x, d_y, and A_c in Table I) for certain discrete values of increased external load. Furthermore, thinning of the film is accompanied by structuring of the density which exhibits, for both values of the molecule-to-surface adsorption strengths, an oscillatory layered behavior (see Figs. 3 and 4) with a period (~ 4 Å) comparable to that observed experimentally.[7(a),31] We note that for a given value of load the film thickness (d_z) for the strongly adsorbing case is smaller than that of the weakly adsorbed film; see Table I. In this context we remark that the (internal) load values corresponding to a specified number of layers (and thus film thickness) calculated by us, are larger than those obtained via surface-force measurements on

hexadecane droplets confined between mica cylinders sliding with respect to each other.[7(a)] Nevertheless, the overall response characteristics of the film to applied load are consistent with the observed ones[7(a),31] and the load values can be influenced by material factors (e.g., solid substrates and molecule-to-surface interaction potentials), by the relative motion of the two confining surfaces (which are stationary in our simulations and are in relative motion in the experiments,[7(a)] and by other factors (such as the simulated hexadecane semidroplet configuration, assumed parallel-plate orientation of the confining solid crystalline substrates, and their static nature,[43] as well as the higher temperature of the simulated system).

In addition to the oscillatory behavior of the segment-density profile across the confined film, and the relation between the magnitude of the load and film thickness (and correspondingly number of layers), the simulations reveal a wealth of structural information pertaining to the molecular conformations and orientations with respect to the bounding solid surfaces and their dependence on distance from the confining crystalline surfaces. In this context we should remark that except for the weak adsorption case under the lowest load (see Table I) all the films which we have investigated are thin enough to be considered as wholly of interfacial character, i.e., full bulk behavior should not be expected for such thin films at any region of the film since their small thickness should not allow the influence of the solid boundaries to fully damp out across the film. Nevertheless, our results indicate that even for such thin films one may distinguish (for certain properties) interfacial characteristics in regions proximal to the solid boundaries from those toward the middle of the film.

Our results show that near the interface the molecules assume a "flattened" shape, and that in the interfacial region two-bond vectors [i.e., $r_{i,i+2}$ ($i \leqslant i \leqslant 14$) connecting two nonadjacent neighboring segments in a molecule] are preferentially aligned parallel to the solid surface. In addition, we observe an enhanced probability for molecular conformations in which one of the chain ends is located at one of the solid-to-liquid interfaces and the other end also adsorbed at the same interface or located further away from it (i.e., toward the middle of the film and beyond), with the latter one more abundant (particularly for the weak adsorption, i.e., $\epsilon_3 = \epsilon_2$, case; in this context, see also Figs. 5 and 6 where profiles of the z location of the molecules' center of mass are shown). The molecular conformations where part (or parts) of a molecule is located at the interface and another part of the same molecule in a region closer to the middle of the film (or beyond it), together with a small number of molecular conformations (occurring when the film thickness is comparable or smaller than the linear dimension of the fully extended molecule) where two ends of a molecule are attached at opposite interfaces, contribute to bridging of the two solid boundaries.

Finally, we have shown that the dynamical mechanisms of thinning, from a three-layer to a two-layer film, for the two molecule-to-surface adsorption strengths are markedly different (see Sec. III C). For the strongly adsorbed system at a critical load the film collapse is sudden and is accompa-

nied by accumulation of stress in the directions parallel to the solid surface plane, mainly due to intermolecular interactions. Subsequently, spreading occurs and the stress is relieved (see Figs. 8, 9, and 10). On the other hand, the transition from a three-layer to a two-layer film for the weakly adsorbed system does not involve stress accumulation (Fig. 11), and is a gradual process (Fig. 7) accompanied by drainage and spreading via diffusion and adsorption of molecules at the film edge (liquid-to-vacuum interface).

ACKNOWLEDGMENTS

Useful conversations with Professor Jacob Israelachvili are gratefully acknowledged. This work was supported by the U.S. Department of Energy, the NSF Tribology Program, Grant No. MSS-8719669, and the AFOSR. Calculations were performed at the Pittsburgh Supercomputer Center supported via a grant of computer time.

APPENDIX: CONDITIONAL FRACTIONAL SEGMENT OCCUPANCIES

The fractional segment (or pseudoatom) occupancy[28(a)] is defined as

$$f_s(z) = (g_s + g_{N-s+1})/2 \quad (1 \leqslant s \leqslant 8), \qquad (A1a)$$

where

$$g_k = \frac{N}{2}\left[\frac{\rho_k(z)}{\rho_{seg}(z)} + \frac{\rho_k(d_z-z)}{\rho_{seg}(d_z-z)}\right] \quad (1 \leqslant k \leqslant 16). \qquad (A1b)$$

Here $N = 16$ is the number of pseudoatoms in the molecule, $\rho_k(z)$ is the density of the kth pseudoatom, and d_z is the normalized thickness of the molecular film (distance between the centers of mass of the solid atoms in the two opposing surface layers of the confining boundaries, from which the sum of solid atomic radii, $\sigma_3 = 0.562\sigma_2$, is subtracted).
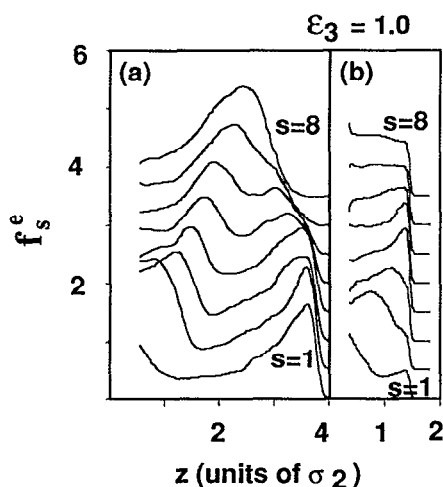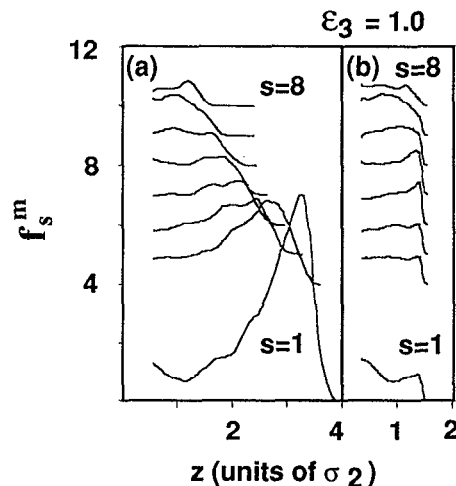

FIG. 13. Conditional fractional occupancies f_s^m, conditioned on one of the middle segments (pseudoatoms 8 or 9) being located in a proximal interfacial region of width $\Delta z_{inter} = 1.1\sigma_2$ from one of the solid surfaces, plotted vs z. Results are given for $L_{ext} = 0.1$ and 1.0 in (a) and (b), respectively.

The two terms in Eq. (A1a) correspond to two symmetrical segments (pseudoatoms) with respect to the middle of the molecule, i.e., segments 1 and 16, 2 and 15, etc. The two terms in Eq. (A1b) correspond to averaging over the two interfaces between the film and the confining solid boundaries. For a homogeneous isotropic distribution of the molecules $\rho_k(z)/\rho_{seg}(z) = 1/N$ and $f_k(z) = 1$ for all z. Thus $f_s(z)$ is a measure of the tendency of pseudoatoms s and/or $16 - s + 1$ to be located in a region centered about z.

In addition to the above occupancy distributions we have analyzed conditional fractional segment occupancy distributions $f_s^{s'}(z)$ which are defined in a manner similar to $f_s(z)$ in Eq. (A1), but conditioned on pseudoatom s' of the molecule being located in the proximal interfacial region, Δz_{inter}. Note that here while for $s \neq s'$ the fractional occupations for segments s and $16 - s + 1$ are combined, those for

FIG. 12. Conditional fractional occupancies f_s^e, conditioned on one of the chain ends (pseudoatoms 1 or 16) being located in a proximal interfacial region of width $\Delta z_{inter} = 1.1\sigma_2$ from one of the solid surfaces, plotted vs z. Results are given for the system characterized by $\epsilon_3 = 1\epsilon_2$ for $L_{ext} = 0.1$ and 1 in (a) and (b), respectively, and in each case for pseudoatoms $1 \leqslant s \leqslant 8$. The curves for $s > 1$ are shifted upwards by 0.5, for clarity.

FIG. 14. Same as Fig. 12, but for the system characterized by $\epsilon_3 = 3\epsilon_2$, for $L_{ext} = 0.1$ and 0.5 in (a) and (b), respectively.
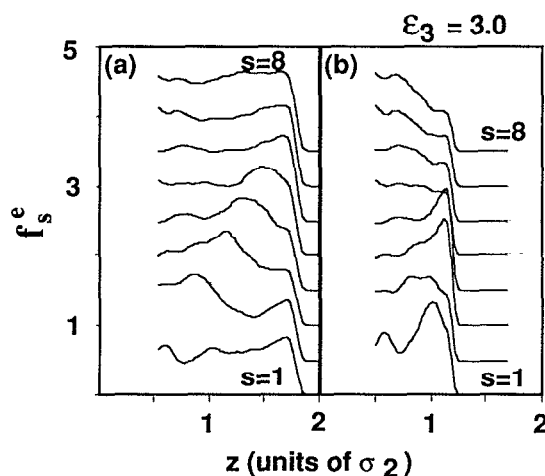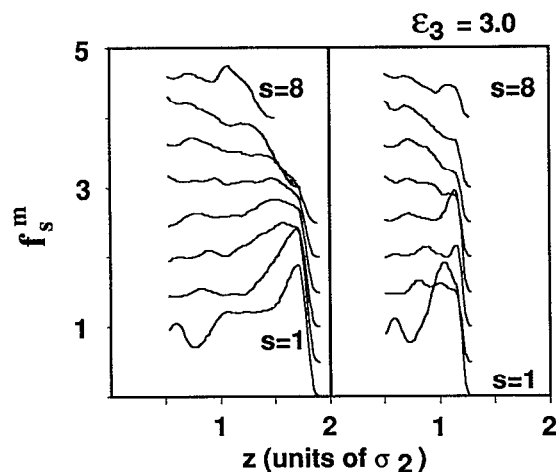
FIG. 15. Same as Fig. 13 but for the system characterized by $\epsilon_3 = 3\epsilon_2$, for $L_{\text{ext}} = 0.1$ and 0.5 in (a) and (b), respectively.

s' and $16 - s' + 1$ are not. For example, if $s' = k, f_s^k(z)$ for $s \neq k$ corresponds to the conditional fractional occupancy of pseudoatoms s and/or $16 - s + 1$ in a region centered about z, while $f_k^k(z)$ gives the fractional occupancy of pseudoatom $16 - k + 1$ in the interfacial region, conditioned on atom k of the molecule being localized there. Such conditional fractional segment occupancy distribution profiles are shown in Figs. 12–15 for the two adsorption strengths, for $s' = 1$ or 16 (i.e., conditioned on finding one of the chain ends in Δz_{inter}), denoted as f_s^e, and for $s' = 8$ or 9 (i.e., conditioned on finding one of the midchain pseudoatoms in Δz_{inter}), denoted as f_s^m. These figures are discussed in Sec. III B.

[1] See U. Landman, W. D. Luedtke, M. Ribarsky, R. N. Barnett, and C. L. Cleveland, Phys. Rev. B **37**, 4637 (1988), and references therein.

[2] See C. L. Cleveland, U. Landman, and R. N. Barnett, Phys. Rev. Lett. **49**, 790 (1982), and references therein.

[3] See J. F. Van der Veen, B. Pluis, and A. W. Denier Van der Gon, in *Kinetics of Ordering at Surfaces*, edited by M. G. Lagully (Plenum, New York, 1990); E. T. Chen, R. N. Barnett, and U. Landman, Phys. Rev. B **40**, 924 (1989); R. N. Barnett and U. Landman, *ibid.* **44**, 3226 (1990), and references therein.

[4] John C. Slattery, *Interfacial Transport Phenomena* (Springer, New York, 1990); *Thin Liquid Films*, edited by I. B. Ivanov (Marcel Dekker, New York, 1988).

[5] See reviews and literature references in (a) J. N. Israelachvili, *Intermolecular and Surface Forces*, (Academic, London, 1985); (b) R. G. Horn, J. Am. Ceram. Soc. **73**, 1117 (1990); (c) R. J. Hunter, *Foundations of Colloid Science*, (Oxford University, Oxford, 1987 and 1989), Vols. 1 and 2; *Fluid Interfacial Phenomena*, edited by C. A. Croxton (Wiley, Chichester, 1986).

[6] See J. N. Israelachvili, P. M. McGuiggan, and A. M. Homola, Science **240**, 189 (1988), and references therein.

[7] (a) J. Van Alsten and S. Granick, Phys. Rev. Lett. **61**, 2570 (1988); (b) H.-W. Hu, G. A. Carson, and S. Granick, Phys. Rev. Lett. **66**, 2578 (1991); S. Granick, Science (in press).

[8] P. A. Thompson and M. O. Robbins, Phys. Rev. A **41**, 6830 (1990); Science **250**, 792 (1990), and references therein; S. Sutton, M. W. Ribarsky, and U. Landman (unpublished); S. Sutton, Ph.D. thesis, Georgia Institute of Technology, 1991 (unpublished).

[9] (a) See articles in *Liquids at Interfaces*, edited by J. Charvolin, J. F. Joanny, and J. Zinn-Justin (North-Holland, Amsterdam, 1990); (b) P.

[9] G. de Gennes, *Scaling Concepts in Polymer Physics* (Cornell University, Ithaca, 1979).

[10] J. N. Israelachvili, Acc. Chem. Res. **20**, 415 (1987); Proc. Natl. Acad. Sci. U.S.A. **84**, 4722 (1987); A. M. Homola, J. N. Israelachvili, P. M. McGuiggan, and M. L. Gee, Wear **136**, 65 (1990).

[11] See reviews by P. K. Hansma and J. Tersoff, J. Appl. Phys. **61**, R1 (1986); R. J. Colton and J. S. Murday, Naval Res. Rev. **40**, 2 (1988); J. S. Murday and R. J. Colton, in *Chemistry and Physics of Solid Surfaces*, edited by R. Vanselow and R. Howe (Springer, Berlin, 1990), Vol. VIII.

[12] C. M. Mate, M. R. Lorenz, and V. J. Novotny, J. Chem. Phys. **90**, 7550 (1989); C. M. Mate and V. J. Novotny, *ibid.* **94**, 8420 (1991).

[13] J. Krim, D. H. Solina, and R. Chiarello, Phys. Rev. Lett. **66**, 181 (1991).

[14] F. F. Abraham, J. Chem. Phys. **68**, 713 (1978); A. Bonissent and F. F. Abraham, *ibid.* **74**, 1306 (1981).

[15] C. A. Croxton, *Statistical Mechanics of Liquid Surfaces* (Wiley, Chichester, 1980).

[16] See a comprehensive review by R. Evans in Ref. 9(a), p. 1.

[17] See references in E. T. Chen, R. N. Barnett, and U. Landman, Phys. Rev. B **40**, 924 (1989).

[18] (a) See P. G. de Gennes in Ref. 9(a), pp. 273 and 293; C. R. Acad. Sci. Paris **305**, 1181 (1987); (b) D. N. Theodorou, Macromolecules **21**, 1400 (1988); (c) see P. G. de Gennes in Ref. 9(a), p. 311; P. G. de Gennes and A. M. Cazabat, C. R. Acad. Sci. Ser. B **310**, 1601 (1990).

[19] M. P. Allen and D. J. Tildesley, *Computer Simulation of Liquids* (Clarendon, Oxford, 1987).

[20] U. Landman, C. S. Brown, and C. L. Cleveland, Phys. Rev. Lett. **45**, 2032 (1980); in *Nonlinear Phenomena at Phase Transitions and Instabilities*, edited by T. Riste (Plenum, New York, 1981).

[21] F. F. Abraham, Adv. Phys. **35**, 1 (1986); J. Vac. Sci. Technol. B **2**, 534 (1984).

[22] J. J. Magda, M. Tirrell, and H. T. Davis, J. Chem. Phys. **83**, 1888 (1985).

[23] J. K. Snook and Van Megan, J. Chem. Phys. **72**, 2907 (1980).

[24] M. Schoen, C. L. Rhykerd, D. J. Diestler, and J. H. Cushman, Science **245**, 1223 (1989).

[25] I. Bitsanis, J. J. Magda, M. Tirrell, and H. T. Davis, J. Chem. Phys. **87**, 1733 (1987).

[26] J. Bitsanis, S. A. Somars, H. T. Davis, and M. Tirrell, J. Chem. Phys. **93**, 3427 (1990).

[27] J. Koplik, J. R. Banavar, and J. F. Willemsen, Phys. Rev. Lett. **60**, 1282 (1988).

[28] For Monte Carlo simulations see (a) M. Vacatello, Do Y. Yoon, and B. Laskowski, J. Chem. Phys. **93**, 779 (1990); (b) S. K. Kumar, M. Vacatello, and Do Y. Yoon, J. Chem. Phys. **89**, 5206 (1988); Macromolecules (in press); G. ten Brinke, D. Ausserre, and G. Hadziioannou, J. Chem. Phys. **89**, 4374 (1988); W. G. Madden, *ibid.* **87**, 1405 (1987); R. Dickman and C. Hall, *ibid.* **89**, 3168 (1988).

[29] I. Bitsanis and G. Hadziioannou, J. Chem. Phys. **92**, 3827 (1990).

[30] See articles in *Computer Simulations of Polymers*, edited by R. J. Roe (Prentice Hall, Englewood Cliffs, NJ, 1991).

[31] H. K. Christenson, D. W. R. Gruen, R. G. Horn, and J. N. Israelachvili, J. Chem. Phys. **87**, 1834 (1987).

[32] U. Landman, W. D. Luedtke, and E. M. Ringer, Wear **153**, 3 (1992).

[33] J. P. Ryckaert and A. Bellmans, Discuss. Faraday Soc. **66**, 95 (1978).

[34] J. H. R. Clarke and D. Brown, J. Chem. Phys. **86**, 1542 (1987).

[35] (a) R. Edberg, G. P. Morriss, and D. J. Evans, J. Chem. Phys. **86**, 4555 (1987); (b) R. Edberg, D. J. Evans, and G. P. Morriss, *ibid.* **84**, 6933 (1986).

[36] For a review see M. F. Van Gunsteren and H. J. C. Berendsen, in *The Physics of Superionic Conductors and Electrode Materials*, edited by J. W. Perram, NATO ASI Ser. B92 (Plenum, New York, 1983), p. 221, and references therein.

[37] (a) M. Fixman, Proc. Natl. Acad. Sci. U.S.A. **71**, 3050 (1974); J. Chem. Phys. **69**, 1527 (1978); (b) N. Go and H. A. Scheraga, Macromolecules **9**, 535 (1976); (c) E. Helfand, J. Chem. Phys. **71**, 5000 (1979); (d) D. Chandler and B. J. Berne, *ibid.* **71**, 5386 (1979); W. F. Van Gunsteren, Mol. Phys. **40**, 1015 (1980).

[38] T. K. Xia, J. Ouyang, M. W. Ribarsky, and U. Landman (unpublished).

[39] S. Leggetter and D. J. Tildesley, Mol. Phys. **68**, 519 (1989).

[40] Thermal desorption studies of alkanes adsorbed on metal surfaces suggest an adsorption energy of ~1 kcal/mol per CH_2 segment [see Q. Dai and A. J. Gellman, Surf. Sci. (in press)]; R. Zhang and A. J. Gellman, J. Phys. Chem. (in press); A. V. Hamza and R. J. Madix, Surf. Sci. **179**, 25 (1987)]. The adsorption energy per CH_2 segment calculated for our system with $\epsilon_3 = 3\epsilon_2$ is comparable to the above value.

[41] M. L. Gee and J. N. Israelachvili, J. Chem. Soc. Faraday Trans. **86**, 4049 (1990).

[42] See articles by P. G. de Gennes in Ref. 9, pp. 273 and 311; M. Schick, in Ref. 9, p. 415, and references therein; D. V. C. Chan and R. G. Horn, J. Chem. Phys. **83**, 5311 (1985); K. F. Mansfield and D. N. Theodorou, Macromolecules **22**, 3143 (1989).

[43] Our recent studies (Ref. 32) of the interaction of a nickel tip exposing a (100) facet with an n-hexadecane film adsorbed on a (100) gold surface show layering of the molecular film in the space between the tip and the surface. Decreasing the distance between the tip and the substrate induced drainage of molecules from the region under the tip, and at high loads, corresponding to small tip-to-surface separation (~5 Å), elastic deformation of the gold surface was observed, and the mechanism of drainage (squeeze-out of molecules) involved dynamic response of the solid substrate.